Small-scale Current Sheets and Associated Switchback Activity in the Inner Heliosphere

Sydney Furman, Alexandros Chasapis, David Malaspina, Peter Tatum, Benjamin Short, Harriet George, Mihailo Martinović

The Astrophysical Journal Letters, 976:L1 (7pp), 2024 November 20 https://doi.org/10.3847/2041-8213/ad8c38

Small-scale Current Sheets and Associated Switchback Activity in the Inner Heliosphere

Sydney Furman[1,2], Alexandros Chasapis[2], David Malaspina[1,2], Peter Tatum[1,2], Benjamin Short[2,3], Harriet George[2], and Mihailo Martinović[4,5]
[1] Astrophysical and Planetary Sciences Department, University of Colorado, 80309 Duane Physics Building, Boulder, CO 80309, USA
[2] Laboratory for Atmospheric and Space Physics, 1234 Innovation Drive, Boulder, CO 80303, USA
[3] Physics Department, University of Colorado, 80309 Duane Physics Building, Boulder, CO 80309, USA
[4] Lunar and Planetary Laboratory, University of Arizona, Tucson, AZ, USA
[5] LESIA, Observatoire de Paris, Université PSL, CNRS, Sorbonne Université, Université de Paris, Meudon, France
Received 2024 August 20; revised 2024 October 26; accepted 2024 October 28; published 2024 November 11

Abstract

Several long-standing theories postulate that turbulent dissipation can heat solar wind protons in situ. Turbulent dissipation can occur via current sheets, which are small-scale structures embedded in the solar wind magnetic field. This study examines the role that switchbacks—intermediate-scale reversals in the interplanetary magnetic field—may play in heating the solar wind by generating current sheets. We explore this possible relationship by analyzing the characteristics of current sheets within and around switchback regions. Previous studies investigated current sheet properties during Parker Solar Probe's first solar encounter, analyzed current sheets using a wide range of statistics, and explored trends that switchbacks follow with radial distance from the Sun. The present study builds on these works by analyzing the distribution and maximum values of solar wind current sheets using the Partial Variance of Increments method and focusing on how these properties correlate with the presence of switchbacks to better understand how switchbacks contribute to current sheet activity. We conclude that there are no increased current sheet populations observed within and around switchbacks, with most current sheets being observed outside switchbacks. We find a consistent distribution of current sheets regardless of whether there is concurrent switchback activity. We also observe that current sheets follow a uniform occurrence rate with increased distance from the Sun, while switchback regions significantly evolve with larger radial distances. Our findings suggest that local turbulence may be responsible for generating solar wind current sheets and does so with the same efficiency inside and outside of switchback regions.

Unified Astronomy Thesaurus concepts: Solar coronal heating (1989); Space plasmas (1544); Solar wind (1534); Solar physics (1476)

1. Introduction

The solar wind is characterized by turbulence, which dissipates magnetic field energy, heating plasma and energizing particles throughout the heliosphere (M. L. Goldstein et al. 1995; C. Y. Tu & E. Marsch 1995; M. K. Verma et al. 1995; R. Bruno & V. Carbone 2013; K. H. Kiyani et al. 2015; D. Verscharen et al. 2019). Energy injected at large scales in the corona is transferred via the turbulent energy cascade to smaller scales, where it is eventually converted into heat and accelerates solar wind particles. Turbulent dissipation occurs throughout the heliosphere, leading to additional heating of the solar wind through several different pathways of energy conversion (B. J. Vasquez et al. 2007b; R. Marino et al. 2008; J. E. Stawarz et al. 2009; R. Bandyopadhyay et al. 2020). One major pathway is intermittent dissipation localized within structures that form as a consequence of turbulence, such as small-scale current sheets. Current sheets are observed to form in turbulence omnipresent throughout the solar wind. Active magnetic reconnection has been associated with such structures (K. T. Osman et al. 2014) and is thought to be a major pathway of dissipation and particle energization.

In order to understand this potential dissipation pathway, we need to examine populations of current sheets and how they evolve throughout the heliosphere. The generation and evolution of current sheets, as well as their contribution to turbulent dissipation, are a topic of intense study (L. F. Burlaga 1969, 1991; B. J. Vasquez et al. 2007a; J. E. Borovsky 2008, 2021; K. T. Osman et al. 2012; A. Chasapis et al. 2017, 2018; F. D. Wilder et al. 2018).

Recent observations by the Parker Solar Probe (PSP) mission have revealed that magnetic field switchback structures—bends in the Sun's magnetic field departing from the Parker spiral—are often present in the solar wind in the inner heliosphere (N. E. Raouafi et al. 2023). Moreover, results from previous studies suggest that they may drive turbulent evolution more so than less-developed structures observed in quieter regions (T. Dudok de Wit et al. 2020; C. S. Hernández et al. 2021). As such, it is compelling to examine whether the number of observed current sheets increases in the vicinity of switchback structures. Addressing this question will help us better understand where and how current sheets are generated in the solar wind. Here, we use in situ observations by PSP (N. J. Fox et al. 2016) to detect current sheets forming in the turbulence of the inner heliosphere (sunward of 60 solar radii, R_S).

In this study, we employ the Partial Variance of Increments (PVI) method to detect current sheets in the near-Sun solar wind plasma, and we examine how their occurrence varies with respect to switchback occurrence. We observe similar current sheet populations within and outside of switchback regions, indicating that current sheets formed within switchback regions are not the dominant population. This observation suggests

different mechanisms, including turbulent intermittency measured throughout the solar wind, are responsible for the generation of most of the current sheet population observed in the inner heliosphere.

2. Data

In this work, we use magnetic field data as measured by NASA's PSP (N. J. Fox et al. 2016). The mission's primary science objectives are to (1) trace the flow of energy that heats the solar corona and accelerates the solar wind; (2) determine the structure and dynamics of the plasma and magnetic fields at the sources of the solar wind; and (3) explore mechanisms that accelerate and transport energetic particles (N. J. Fox et al. 2016). We use data from the outboard fluxgate magnetometer, which is part of the FIELDS (S. D. Bale et al. 2016) instrument suite and measures low-frequency magnetic fields (DC to ∼146 Hz) in the radial–tangential–normal (RTN) coordinate system. We measure solar wind proton velocity using the Solar Probe Cup in the SWEAP instrument suite to establish an ion gyroradius against which we compare the characteristic temporal and spatial scales of the current sheets we examine (J. C. Kasper et al. 2016; A. W. Case et al. 2020).

Each time PSP reaches perihelion during its orbits, we count an encounter. We use data from Encounters 4, 6, and 13 to cover a representative range of radial distances sampled during the mission. During those encounters, the PSP spacecraft perihelia were 27.9, 20.4, and 13.3 R_S, respectively, allowing us to investigate how current sheet spatial density varies with distance to the Sun. Specifically, we examine 360 hr of data from Encounter 4 (spanning 2020 January 22 to 2020 February 5), 354 hr from Encounter 6 (spanning 2020 September 18 to 2020 October 4), and 312 hr from Encounter 13 (spanning 2022 August 30 to 2022 September 11). In each case, the observation intervals are centered on perihelion, where the data sample rate is higher, allowing for a more precise analysis.

We used magnetic field data to calculate PVI index values, the scale-dependent kurtosis (SDK), and the normalized deflection parameter z, used for estimating switchback occurrence, as described in the next section.

3. Methodology

For this study, we detect current sheets by employing the PVI method, which is described in detail by A. Greco et al. (2017). This approach quantifies sharp changes of the magnetic field associated with regions of strong current, typically related to intermittent structures formed in turbulence. Past studies have shown peaks of the PVI index can be used to identify current sheets in the turbulence of the solar wind (A. Greco et al. 2009; S. Servidio et al. 2011; D. M. Malaspina et al. 2013). The PVI index is calculated as follows:

$$\mathrm{PVI}(s, \tau) = \frac{|\Delta B(s, \tau)|}{\sqrt{\langle |\Delta B(s, \tau)|^2 \rangle_T}}, \quad (1)$$

over time s, and where ΔB is the magnitude of the the change of the vector magnetic field over time lag τ. We use a time lag $\tau = 1$ s, which corresponds to approximately a few times the ion inertial scales at the radial distances sampled here (R. Chhiber et al. 2020). We use this time lag because we focus on small-scale current sheets close to the lower end of the inertial range of the solar wind turbulence, where dissipative processes begin to become important.

We calculate the variance of the measured magnetic field fluctuations over a 1 hr rolling window ($T = 1$ hr), which corresponds to the typical correlation timescale of magnetic field fluctuations for the range of radial distances of these encounters, as estimated by previous studies using PSP observations in the inner heliosphere (R. Bandyopadhyay et al. 2020; T. N. Parashar et al. 2020). The resulting calculation of the PVI index for a 6 hr period from Encounter 4 at approximately 28 R_S is shown in Figure 1(b). We see strong variability over time with some periods, such as the 1 hr long interval shaded in red and marked as Region 1, containing several strong PVI spikes indicating the presence of current sheets. Other periods, such as the interval shaded in green and marked as Region 2, are calmer with fewer and less intense current sheets.

We set a PVI value of five as our threshold for defining structures since we focused on strong current sheets that typically have been found to be associated with heating and dissipation (A. Greco et al. 2008; K. T. Osman et al. 2010; N. Sioulas et al. 2022). We define a current sheet event where the local value of the PVI index exceeds our threshold, $\mathrm{PVI} > 5$. We record the maximum value of the PVI index within each event as the local PVI index of the detected current sheet. We also determine the number of such current sheets observed per hour during each encounter to analyze their distribution.

We note that this method does not explicitly consider the shear angle of the magnetic field, which contributes to the value of the PVI index. Such approaches have been used to study discontinuities in the solar wind (V. Zhdankin et al. 2012), while more advanced methods, including those used by B. J. Vasquez et al. (2007a), give further insight into the physics of the detected current sheets.

Since switchbacks are known to be associated with regions of turbulence with higher amplitudes of turbulent fluctuations (T. Dudok de Wit et al. 2020), as well as a higher turbulent energy cascade rate (C. S. Hernández et al. 2021), our study examines the connection between intervals of solar wind that contain switchbacks and the statistical properties of current sheet populations. Recent work indicates that switchback structures are associated with different source regions on the Sun, with different compositions and turbulence conditions evolving distinctly from the ambient solar wind (S. D. Bale et al. 2021; L. D. Woodham et al. 2021; J. Huang et al. 2023).

To detect switchbacks, we use the normalized deflection method as defined by T. Dudok de Wit et al. (2020), $z = \frac{1}{2}(1 - \cos\alpha)$, where α is the deflection angle of the solar wind from the Parker spiral. For this work, PSP is defined to be within a switchback when $z > 0.5$ (T. Dudok de Wit et al. 2020), which corresponds to a magnetic field deflection larger than 90° from the Parker spiral. Our threshold differs from T. Dudok de Wit et al. (2020) as we focus on locating switchbacks associated with large deviations from the Parker spiral, whereas T. Dudok de Wit et al. (2020) set a threshold of $z < 0.05$ to identify quiescent regions of pristine solar wind. Figure 1(c) shows the normalized deflection parameter as a function of time over a 6 hour period during Encounter 4. As we can see in Figure 1, periods of significant switchback activity may be associated with periods containing many current sheets, for example, in Region 1, shaded in red. When

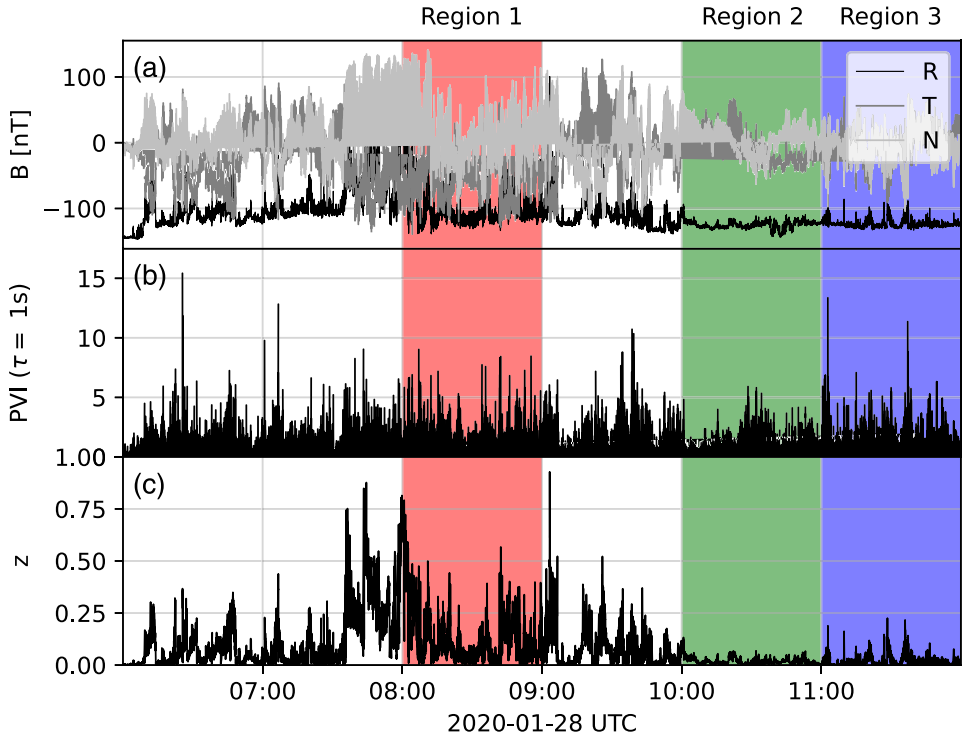

Figure 1. An example of the magnetic field (B), PVI index, and normalized deflection parameter (z) over a 6 hr period during PSP's fourth solar encounter. B is shown in panel (a) in RTN coordinates, the PVI index is shown in panel (b), and the normalized deflection parameter is shown in panel (c). Three regions are shown, marked as Region 1, 2, and 3, shaded in red, green, and blue, respectively. Region 1 shows switchback activity along with many current sheets. Region 2 is less turbulent, without any switchbacks, and few current sheets are detected. Region 3 shows minimal switchbacks, but many current sheets are present.

no switchback activity is present, in some cases, there are few detected current sheets, such as in Region 2, shaded in green. However, in other cases, such as in Region 3, shaded in blue, there is a lack of switchback activity, but a substantial number of current sheets are present, suggesting that these current sheets were generated by a mechanism not associated with switchback turbulence. The three highlighted regions are all 1 hour time periods.

While the PVI method used here uses a single fixed scale, current sheet populations are associated with increased intermittency at small scales, an important indicator of turbulent dissipation (A. Chasapis et al. 2018). Such increased intermittency has been previously observed in solar wind turbulence (L. Sorriso-Valvo et al. 1999; R. Chhiber et al. 2018, 2021) and would be consistent with the regions in Figure 1 that show a larger number of current sheets.

We estimate the intermittency at different scales by calculating the SDK, written as κ, for the three regions identified above. As a normalized quantity, kurtosis is useful for highlighting the tails of Gaussian distributions. Current sheets generated by local turbulence appear in these tails as values $\kappa(\tau) > 3$. This helps us establish whether the current sheets detected using the PVI method are associated with increased intermittency at small scales. To calculate the SDK of each component of the magnetic field,

$$\kappa(\tau) = \frac{\langle \delta B_i^4 \rangle}{\langle \delta B_i^2 \rangle^2} \tag{2}$$

where $\delta B_i = B_i(t) - B_i(t+\tau)$, τ is the same time lag used in Equation (1), and $i = R, T, N$ for each of the components of the magnetic field vector. For random Gaussian fluctuations, we expect the SDK to have a value of $\kappa(\tau) = 3$, while higher values correspond to sharp changes in the magnetic field associated with intermittent structures such as current sheets (R. Chhiber et al. 2018).

The SDK for the three shaded regions from Figure 1 is shown in the three separate panels of Figure 2. Each panel shows the SDK for all three magnetic field components. We observe a gradual increase of the kurtosis for all three intervals as we move from larger to smaller time lags—from right to left on each panel—starting from values around $\kappa(\tau) = 3$ at large scales, consistent with random Gaussian fluctuations, with a gradual increase to a peak as we go to smaller scales at lags corresponding to about $\tau = 1$ s. This indicates sharp jumps in the magnetic field are present at those scales due to increased occurrence of intermittent structures. This is in agreement with previous studies carried out in the solar wind at 1 au (R. Chhiber et al. 2018; O. W. Roberts et al. 2022).

The increased intermittency indicated by the large values of the SDK can be attributed to the small-scale structures commonly observed in solar wind turbulence, such as the ones typically detected by the PVI method. This demonstrates that the use of the PVI index with a lag of 1 s, in this case, is a good measure of intermittency at those scales and a good proxy for the presence of small-scale current sheets.

Comparing the three intervals, we note that Region 1 and Region 3, the ones with higher values of the PVI index, as shown in Figure 1(b), also show the largest values of the SDK for all three components of the magnetic field, confirming the earlier determination that there are relatively more current sheets in those regions compared to Region 2.

Finally, it is interesting to note the significant anisotropy between the SDK of the magnetic field fluctuations along the radial direction of the solar wind and the other two

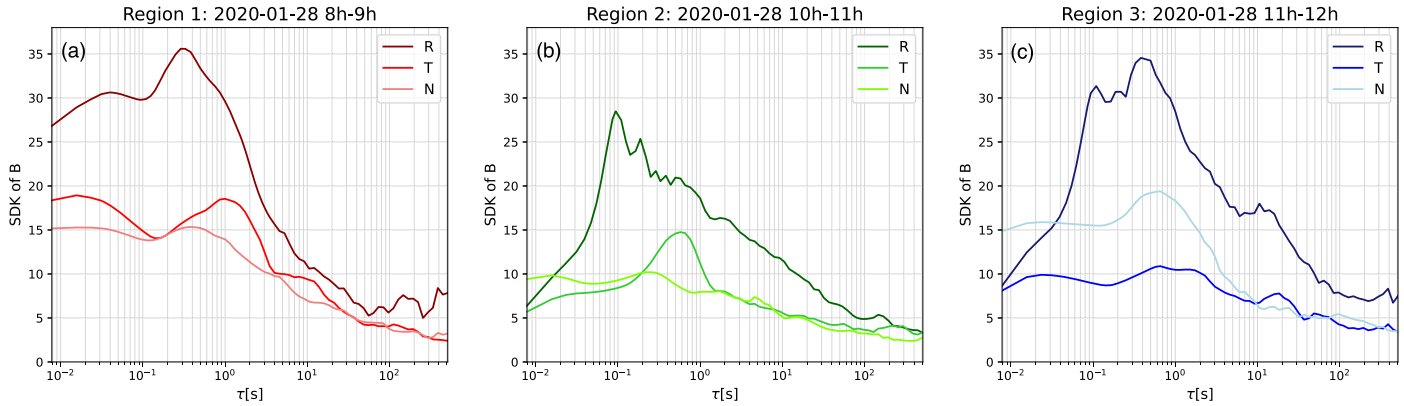

Figure 2. SDK for each component of the magnetic field measured by PSP during the three intervals highlighted in Figure 1. Each panel corresponds to a 1 hr region, with Region 1 in panel (a), Region 2 in panel (b), and Region 3 in panel (c). Each line corresponds to one of the magnetic field vector components measured in RTN coordinates. The x-axis shows the time lag value in seconds, corresponding to the scale at which the magnetic field increments were calculated.

components. For the heliocentric distances involved, the radial direction falls generally within a few degrees of the Parker spiral angle. This feature is present through all three intervals. It should also be noted that the local scale-dependent mean field direction may deviate from the Parker spiral direction (J. E. Borovsky 2010), and this aspect invites further investigation. Although beyond the scope of this work, further investigation would offer a compelling window into the anisotropic distribution and orientation of intermittent structures of the solar wind in the inner heliosphere, as has been the focus of similar work at 1 au (A. Chasapis et al. 2020; O. W. Roberts et al. 2022).

In the case study shown in Figure 1, we find current sheet populations associated with both high (Region 1 in red) and low (Region 3 in blue) normalized deflection parameters z, and a region with few current sheets associated with low normalized deflection parameter z (Region 2 in green).

In Region 1, we observe high values of the normalized deflection parameter, indicating the presence of switchback activity and coinciding with large spikes of the PVI index associated with current sheets. This is corroborated by the large values of the SDK shown in Figure 2(a). Region 2 maintains low values of the normalized deflection and a PVI index with few large spikes observed. In Region 3, we see significant activity in the PVI index, with several large spikes indicating the presence of strong current sheets, along with a higher SDK, similar to Region 1. However, in Region 3, the normalized deflection parameter stays low compared to Region 1. Some limited switchback activity is observed but is greatly reduced compared to Region 1. This suggests that any additional energy injected into the turbulent cascade by switchbacks does not significantly increase the generation of intermittent turbulent structures. We should note that these low deflection angles could be in proximity to switchbacks, as we do not necessarily expect a large deflection, depending on the direction the spacecraft slices through each structure. In this case, these current sheets could still be associated with the vicinity of switchback structures (M. M. Martinovic et al. 2021).

4. Statistics of Current Sheet Populations

To understand whether there is a systematic link between current sheet occurrence and switchback occurrence, we expanded this analysis to a larger set of PSP observations. The data set, described in Section 2, encompasses three separate encounters by PSP. We evaluate the presence of switchback activity using the normalized deflection parameter z and use the PVI index as a proxy for intermittent current sheets.

As described in Section 3, we consider intervals where the local PVI index exceeds our threshold (PVI > 5) as a current sheet and register the largest PVI value measured during each current sheet event, defined as the time interval that the PVI time series exceeds the set threshold. For each local maximum of the PVI index, we also register the local value of the normalized deflection z to note the association with switchback activity, with larger values of z corresponding to larger deflections of the solar wind magnetic field.

Figure 3 shows the distribution of current sheet occurrences as a function of the maximum values of the PVI for each current sheet and the corresponding value of normalized deflection z. Each grid bin is colored using the raw number of current sheet occurrences in that bin, while the fractional occupancy of each bin, normalized to the total number of current sheets in a given column, is indicated by a number in that bin. Data from all three encounters studied are included in this distribution.

Most of the detected current sheets occur when z is close to 0, indicating a relative abundance of current sheets when the magnetic field is locally aligned with the Parker spiral. Relatively few current sheets are identified when z approaches 1, indicating a lack of small-scale current sheets coinciding with large reversals of the field.

In the above analysis, we focus on current sheets detected simultaneously with large deflections of the magnetic field. However, current sheets associated with switchbacks may be observed in regions surrounding switchback patches but not exactly coinciding with a large deflection parameter, leading to an offset between the peaks of the PVI time series and z.

To account for this potential effect, we calculate the percentage of time spent with $z > 0.5$ within each 1 hr window of data as a proxy for switchback activity within that time window. Figure 4 shows the number of current sheet occurrences as a function of the percentage of each 1 hr window where $z > 0.5$ and the maximum PVI for each current sheet. Each grid bin is colored using the raw number of current sheet occurrences in that bin, while the fractional occupancy of each bin, normalized to the total number of current sheet occurrences in a given column, is indicated by a number in that bin.

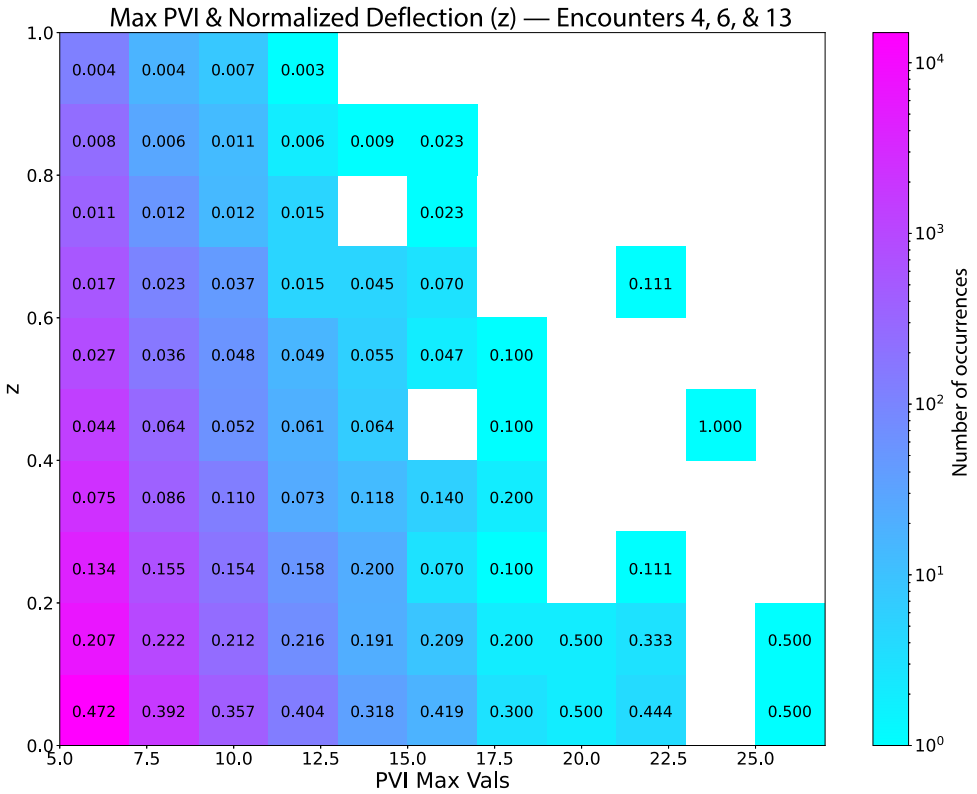

Figure 3. A two-dimensional histogram relating PVI maxima to local normalized deflection values. Pink boxes indicate more events occurring with the associated z and PVI values than the values associated with the blue boxes. Each column has been normalized to one, making the values in each box the quotient of the total events in each box and the total events in the corresponding column. White boxes indicate no events were detected with those associated PVI and z values. The color bar shows the raw number of events detected.

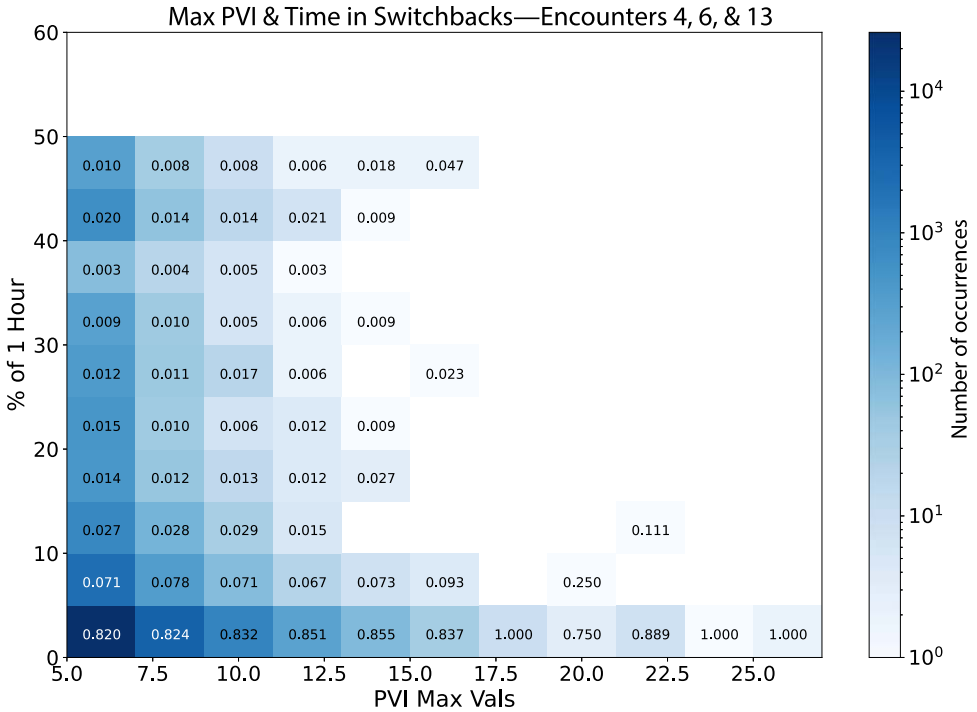

Figure 4. A two-dimensional histogram relating PVI maxima and the percent of the hour during which they occurred that PSP spent in a switchback region. Deeper blues correspond to a higher frequency of events. Similar to the above two-dimensional histogram, each column has been normalized to one. White boxes indicate no events were detected with those associated PVI and z values. The color bar shows the raw number of events detected.

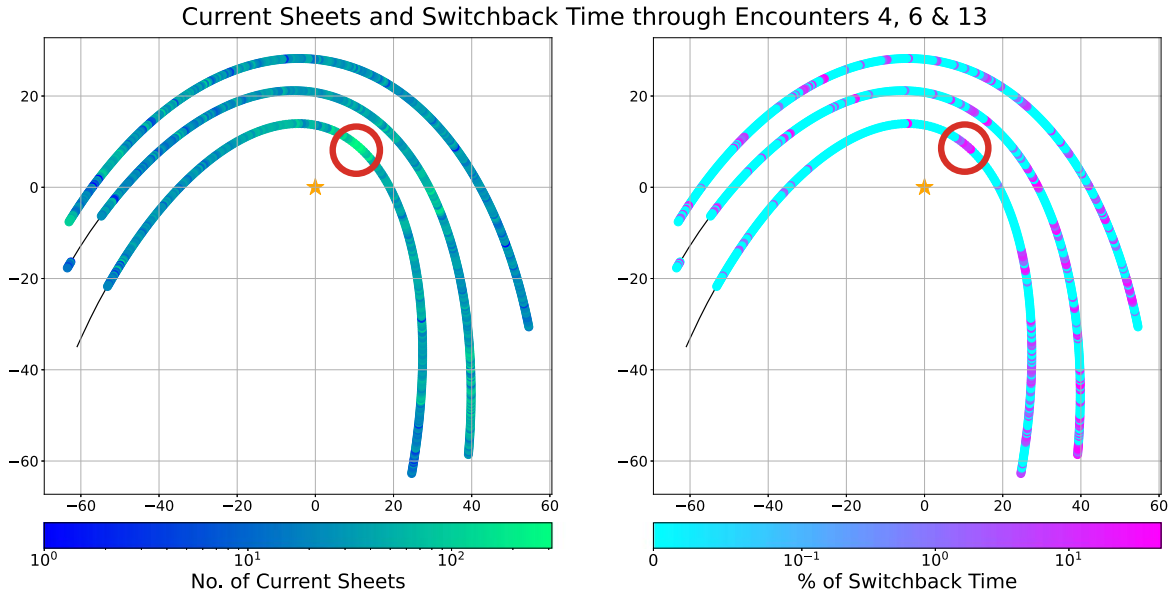

Figure 5. Orbital plots showing how the number of switchback regions and current sheets changes as PSP orbits the Sun. Each line is one of the three encounters examined here. The horizontal and vertical axes show the spacecraft position in X and Y heliocentric coordinates, respectively, roughly corresponding to the plane of the ecliptic. The left panel shows the number of current sheets within a 1 hr window for each point of the orbit. The right panel shows the percentage of time with normalized deflection value $z > 0.5$, indicating stronger switchback activity. A small region circled in red indicates a CME encountered by PSP.

Strong current sheets (largest PVI) are more prevalent when normalized deflection is low. This corresponds to behavior like Region 3 in the case study shown earlier in Figure 1. A smaller population of current sheets appears when $z > 0.5$ for more than 35% of each hour, indicating an association between these current sheets and switchback activity, similar to Region 1 in Figure 1. However, this set of current sheets is subdominant, making up approximately 3% of the total current sheets detected, indicating that additional energy injected into the turbulent cascade by switchbacks does not lead to a large increase in the generation of current sheets.

We note the interesting persistence of a significant population of current sheets that occurs when the local field is close to radial but are also within regions of low deflection parameter solar wind. These structures could be generated by the local turbulence (R. Chhiber et al. 2020), away from switchback activity, despite the lower amplitudes of turbulence that some studies have observed in those quiet regions of the solar wind (T. Dudok de Wit et al. 2020). Alternatively, intermittent structures could also be generated in other regions of solar wind and advected into low deflection parameter solar wind regions where they are observed. However, if a current sheet source region is associated with switchback activity, one would expect larger numbers of current sheets near large deflections of the field ($z > 0.5$), which are not observed here.

Finally, we examine the evolution of the current sheet population throughout the orbit of the spacecraft during the three encounters included in this analysis. Figure 5 shows (on the left) the number of current sheets detected within each 1 hr window throughout the orbit and (on the right) the percentage of time with normalized deflection $z > 0.5$.

The number of current sheets per hour is patchy but homogeneously distributed throughout each orbit and does not show any clear connection to the orbital distribution of switchback activity. This is consistent with the results presented above, where the number of observed current sheets is not related to any clear switchback activity.

Furthermore, no apparent spatial or radial trend in the number of current sheets observed is present, suggesting that most of the detected current sheets are generated by the local turbulence throughout the solar wind or that they are consistently advected outward and persist throughout the heliosphere.

We note an encounter with a coronal mass ejection (CME) that occurred on 2020 September 6, marked with a red circle in both panels of Figure 5. There, a significant increase in the number of current sheets detected per hour is present, coinciding with significant deflection of the solar magnetic field, as shown by the percentage of time of high normalized deflection. In this case, we consider both the large number of current sheets and the solar wind magnetic field deflection to be caused by the passage of the CME. It is the only such event within this data set.

5. Discussion

This study explores questions stemming from PSP's goal to examine mechanisms that accelerate and transport energetic particles (N. J. Fox et al. 2016). Specifically, we investigate the possible role of turbulence as generated through switchbacks in manifesting current sheets in the solar wind throughout the inner heliosphere. We examine populations of small-scale current sheets observed by PSP with regard to their association with switchback activity. We use the PVI index to detect current sheets and the normalized deflection angle of the magnetic field to indicate switchback activity.

As shown in Figure 3, most detected current sheets are associated with low values of normalized deflection and thus minimal switchback activity. Most current sheets, and almost all high-PVI current sheets, occurred when the normalized deflection was small. Only a small fraction of the total current sheet population coincided with large normalized deflection and thus higher levels of switchback activity.

We examine current sheet PVI values with respect to the fraction of each hour that contained large normalized deflection of the magnetic field. This is done to control for current sheets

that may occur near significant switchback activity but may not occur immediately adjacent to a large magnetic field deflection. In this analysis, most current sheets occur in regions of small normalized deflection angle. A smaller population of current sheets was detected when normalized deflection $z > 0.5$ was observed for more than 35% of a given 1 hr window. This subset of current sheets, which makes up approximately 3% of the total number of observed current sheets, may be associated with switchback structures.

6. Conclusion

In conclusion, our results show that most of the current sheets we observe in this study are associated with low normalized deflection values. This suggests that despite reports of enhanced turbulent energy transfer within switchbacks (C. S. Hernández et al. 2021) and higher overall fluctuation amplitudes (T. Dudok de Wit et al. 2020), the current sheets observed within and around switchback regions are not the dominant population, with most current sheets being observed outside switchbacks. This indicates that the mechanisms that produce the majority of the observed current sheets are active both inside and outside switchback regions. The turbulent energy cascade, generating intermittency throughout the solar wind, could account for the formation of these structures, along with other mechanisms active in the inner heliosphere. Finally, no notable radial evolution of the distribution of current sheet occurrence was observed, suggesting either constant generation or constant advection of these structures throughout the solar wind.

Further study as the PSP spacecraft reaches deeper into the inner heliosphere, and in conjunction with Solar Orbiter, will help us further understand the generation and evolution of small-scale intermittent structures in solar wind turbulence, as well as their role in dissipation and heating. More detailed analysis of the properties of the detected current sheets, such as determining their normal direction, thickness, and waiting time distribution, similar to work carried out at 1 au (B. J. Vasquez et al. 2007a), would help expand our understanding of the physics of such structures and their contribution to the turbulent solar wind.

Upcoming missions such as HelioSwarm and Plasma Observatory will take advantage of multipoint, multiscale measurements to comprehensively examine the role and nature of intermittent structures in solar wind turbulence.

Acknowledgments

Parker Solar Probe was designed, built, and is now operated by the Johns Hopkins Applied Physics Laboratory as part of NASA's Living with a Star (LWS) program (contract NNN06AA01C). Support from the LWS management and technical team has played a critical role in the success of the Parker Solar Probe mission. B.M.S. acknowledges support from NASA grant No. 80NSSC23K1627. A.C. acknowledges support from NASA Grants 80NSSC21K0454, 80NSSC22K0688, and 80NSSC24K0172.

ORCID iDs

Sydney Furman https://orcid.org/0009-0001-5818-2682
Alexandros Chasapis https://orcid.org/0000-0001-8478-5797
David Malaspina https://orcid.org/0000-0003-1191-1558
Peter Tatum https://orcid.org/0000-0002-4626-4656
Benjamin Short https://orcid.org/0000-0003-3945-6577
Harriet George https://orcid.org/0000-0002-3715-4623
Mihailo Martinović https://orcid.org/0000-0002-7365-0472

References

Bale, S. D., Goetz, K., Harvey, P. R., et al. 2016, SSRv, 204, 49
Bale, S. D., Horbury, T. S., Velli, M., et al. 2021, ApJ, 923, 174
Bandyopadhyay, R., Goldstein, M. L., Maruca, B. A., et al. 2020, ApJS, 246, 48
Borovsky, J. E. 2008, JGRA, 113, A08110
Borovsky, J. E. 2010, JGRA, 115, A09101
Borovsky, J. E. 2021, FrASS, 8, 131
Bruno, R., & Carbone, V. 2013, LRSP, 2, 4
Burlaga, L. F. 1969, SoPh, 7, 54
Burlaga, L. F. 1991, JGR, 96, 5847
Case, A. W., Kasper, J. C., Stevens, M. L., et al. 2020, ApJS, 246, 43
Chasapis, A., Matthaeus, W. H., Bandyopadhyay, R., et al. 2020, ApJ, 903, 127
Chasapis, A., Matthaeus, W. H., Parashar, T. N., et al. 2017, ApJL, 844, L9
Chasapis, A., Matthaeus, W. H., Parashar, T. N., et al. 2018, ApJL, 856, L19
Chhiber, R., Chasapis, A., Bandyopadhyay, R., et al. 2018, JGRA, 123, 9941
Chhiber, R., Goldstein, M. L., Maruca, B. A., et al. 2020, ApJS, 246, 31
Chhiber, R., Matthaeus, W. H., Bowen, T. A., & Bale, S. D. 2021, ApJL, 911, L7
Dudok de Wit, T., Krasnoselskikh, V. V., Bale, S. D., et al. 2020, ApJS, 246, 39
Fox, N. J., Velli, M. C., Bale, S. D., et al. 2016, SSRv, 204, 7
Goldstein, M. L., Roberts, D. A., & Matthaeus, W. H. 1995, ARA&A, 33, 283
Greco, A., Chuychai, P., Matthaeus, W. H., Servidio, S., & Dmitruk, P. 2008, GeoRL, 35, L19111
Greco, A., Matthaeus, W. H., Perri, S., et al. 2017, SSRv, 214, 1
Greco, A., Matthaeus, W. H., Servidio, S., Chuychai, P., & Dmitruk, P. 2009, ApJL, 691, L111
Hernández, C. S., Sorriso-Valvo, L., Bandyopadhyay, R., et al. 2021, ApJL, 922, L11
Huang, J., Kasper, J. C., Fisk, L. A., et al. 2023, ApJ, 952, 33
Kasper, J. C., Abiad, R., Austin, G., et al. 2016, SSRv, 204, 131
Kiyani, K. H., Osman, K. T., & Chapman, S. C. 2015, RSPTA, 373, 20140155
Malaspina, D. M., Newman, D. L., Willson, L. B., et al. 2013, JGRA, 118, 591
Marino, R., Sorriso-Valvo, L., Carbone, V., et al. 2008, ApJL, 677, L71
Martinovic, M. M., Klein, K. G., Huang, J., et al. 2021, ApJ, 912, 28
Osman, K. T., Matthaeus, W. H., Gosling, J. T., et al. 2014, PhRvL, 112, 215002
Osman, K. T., Matthaeus, W. H., Greco, A., & Servidio, S. 2010, ApJL, 727, L11
Osman, K. T., Matthaeus, W. H., Wan, M., & Rappazzo, A. F. 2012, PhRvL, 108, 261102
Parashar, T. N., Goldstein, M. L., Maruca, B. A., et al. 2020, ApJS, 246, 58
Raouafi, N. E., Matteini, L., Squire, J., et al. 2023, SSRv, 219, 8
Roberts, O. W., Alexandrova, O., Sorriso-Valvo, L., et al. 2022, JGRA, 127, e2021JA029483
Servidio, S., Greco, A., Matthaeus, W. H., Osman, K. T., & Dmitruk, P. 2011, JGRA, 116, A09102
Sioulas, N., Velli, M., Chhiber, R., et al. 2022, ApJ, 927, 140
Sorriso-Valvo, L., Carbone, V., Veltri, P., Consolini, G., & Bruno, R. 1999, GeoRL, 26, 1801
Stawarz, J. E., Smith, C. W., Vasquez, B. J., Forman, M. A., & MacBride, B. T. 2009, ApJ, 697, 1119
Tu, C. Y., & Marsch, E. 1995, SSRv, 73, 1
Vasquez, B. J., Abramenko, V. I., Haggerty, D. K., & Smith, C. W. 2007a, JGRA, 112, A11102
Vasquez, B. J., Smith, C. W., Hamilton, K., MacBride, B. T., & Leamon, R. J. 2007b, JGRA, 112, A07101
Verma, M. K., Roberts, D. A., & Goldstein, M. L. 1995, JGR, 100, 19839
Verscharen, D., Klein, K. G., & Maruca, B. A. 2019, LRSP, 16, 5
Wilder, F. D., Ergun, R. E., Burch, J. L., et al. 2018, JGRA, 123, 6533
Woodham, L. D., Horbury, T. S., Matteini, L., et al. 2021, A&A, 650, L1
Zhdankin, V., Boldyrev, S., & Mason, J. 2012, ApJL, 760, L22